Results in Engineering 28 (2025) 107111

Contents lists available at ScienceDirect

Results in Engineering

journal homepage: www.sciencedirect.com/journal/results-in-engineering

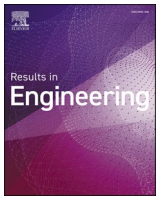

Waste polyethylene-coated fabrics for dual-mode interfaces triboelectrification for self-powered sensors

Kushal Ruthvik Kaja [a], Sugato Hajra [a,*], Swati Panda [a], Mohamed Belal [a], Sangwoo Nam [a], Phakkhananan Pakawanit [b], Basanta Kumar Panigrahi [c], Hamideh Khanbareh [d], Chris Bowen [d], Jaesok Yu [a,*], Hoe Joon Kim [a,*]

[a] Department of Robotics and Mechatronics Engineering, Daegu Gyeongbuk Institute of Science and Technology, Daegu 42988, Republic of Korea
[b] Synchrotron Research and Applications Division, Synchrotron Light Research Institute, Nakhon Ratchasima 30000, Thailand
[c] Deaprtment of Electrical Engineering, Siksha O Anusandhan University, Bhubaneswar 751030, India
[d] Department of Mechanical Engineering, University of Bath, Bath BA2 7AY, UK

ARTICLE INFO

Keywords:
Waste textile
Triboelectric
Solid–solid
Liquid-solid

ABSTRACT

The reuse of waste cotton textiles and coating them with recycled polyethylene provides a route to improve environmental sustainability, reducing our landfill burden and supporting the circular economy through effective implementation of the 3Rs: Reduce, Reuse, and Recycle. This approach extends material life and minimizes resource consumption. This study presents a sustainable strategy for energy harvesting and sensor applications by repurposing worn-out cotton textiles that are coated with recycled polyethylene via a simple immersion method. The modified textiles are integrated into two triboelectric nanogenerator (TENG) configurations: a solid–solid TENG (S–S TENG) and a liquid–solid TENG (L–S TENG). The S–S TENG, paired with a polydimethylsiloxane (PDMS) elastomer, achieves a peak output of 250 V, 1.01 μA, and a power output of 83.7 μW at 2 Hz when subject to a 5 N compression. The device exhibits long-term stability and charges a 10 μF capacitor to 3.3 V, with sufficient energy to power light-emitting diodes (LEDs). For the L–S TENG, deionised water droplets interacting with the polyethylene-coated surface generate up to 45 nW for a 50 MΩ load, with a saturated charge of 1.3 nC. When used as a sensor, the device is employed in real-time motion tracking, integrated with an artificial neural network, and in milk adulteration detection. These results demonstrate a low-cost, flexible, and eco-friendly platform for multifunctional energy harvesting and self-powered sensing, advancing circular economy principles and enabling new applications in healthcare, food safety, and wearable electronics.

1. Introduction

The rapid expansion of the textile industry has led to a significant accumulation of waste cotton textiles, posing both environmental and economic challenges [1]. Cotton cloth, which is composed primarily of natural cellulose, is widely used due to its comfort and breathability. However, its disposal, after use, contributes to landfill burden and resource wastage [2]. Reusing waste cotton textiles not only addresses the issue of textile waste management but also opens avenues for new value-added applications [3,4]. However, cotton fabrics are inherently hydrophilic, which limits their utility in advanced functional materials. Surface modification techniques, in particular those that convert hydrophilic cotton to hydrophobic cotton, have gained attention for enhancing the performance and durability of cotton-based materials [5,6]. By introducing hydrophobicity, by employing chemical coatings and plasma treatments, the surface energy of cotton cloth is reduced, thereby imparting water repellence and improving resistance to environmental factors [7,8]. Such modifications not only extend the lifespan of cotton textiles but also enable their integration into emerging technologies, including energy harvesting and sensor devices.

Triboelectric nanogenerators (TENGs) have emerged as a promising technology for harvesting mechanical energy from ambient sources, such as human motion, vibrations, and environmental stimuli [9–15]. TENGs operate on the principle of contact electrification and electrostatic induction, whereby two materials with different triboelectric properties are able to generate electrical charges when subject to repeated contact and separation events [16–19]. Waste cotton textiles, when appropriately modified to enhance their triboelectric

* Corresponding authors.
E-mail addresses: sugatohajra@dgist.ac.kr (S. Hajra), jaesok.yu@dgist.ac.kr (J. Yu), joonkim@dgist.ac.kr (H.J. Kim).

https://doi.org/10.1016/j.rineng.2025.107111
Received 5 August 2025; Received in revised form 31 August 2025; Accepted 3 September 2025
Available online 5 September 2025

performance, serve as excellent candidates for the tribopositive layer in TENG devices. The transformation of cotton from a hydrophilic to a hydrophobic material not only improves its triboelectric output by reducing charge dissipation but also enhances its mechanical robustness and environmental stability. Recently, Sugato et al. fabricated a TENG using bathroom waste and fluorinated ethylene propylene (FEP) as a triboelectric layer. When operating in single-electrode mode, the device generated an output of 19 V and 8 μA [20]. Similarly, Navaneeth and team have recently utilized discarded medical plastic to construct a high-performance TENG that achieved an output of 508 V and 105 μA [21]. Another study by Panda et al. employed laboratory waste to create a TENG operating in a single-electrode mode, with outputs of 220 V and 25 μA. This device demonstrated a capability to harness mechanical energy from various natural stimuli, including wind, water droplets, and human motion [22]. In 2020, Xu et al. made notable progress in liquid–solid TENG (L-S TENG) research by creating a droplet energy generator (DEG) that utilizes water droplets interacting with a polytetrafluoroethylene (PTFE) surface. This design achieved a remarkable peak power density of 50.1 W m^{-2} when connected to a 332.0 kΩ load, marking a major advancement in liquid–solid energy harvesting and prompting an increased interest in the field [23]. However, in most cases, the PTFE was utilized as a solid layer, and the potential use of waste-based textiles as a solid layer was not explored [24,25]. As a result, this study supports the utilization of a waste-based solid layer to promote the circular economy and sustainable solutions for waste-to-energy conversion. Mao et al. laid out the design of a fully yarn-based TENG–supercapacitor textile based on PTFE yarn wrapped PDMS/MnO_2 nanowire hybrid elastomer for wearable energy harvesting and storage, delivering 380 V output and powering 200 LEDs with high flexibility, durability, and integration ease [26]. Liu et al. developed a 3D yarn-interlocked hybrid nanogenerator textile that delivers up to 400 V output and 91.6 mW m^{-2} power density, enabling durable, self-powered wearable devices for continuous biomechanical energy harvesting and sensing [27]. Tao et al. designed an all-yarn-based TENG–ASC pressure-sensitive sensor integrating energy harvesting, storage, and sensing that delivers ~3.5 V output, 2.14 mW m^{-2} power density, 3.2 mWh cm^{-3} energy density, and 30.3 kPa^{-1} sensitivity, offering a highly flexible, miniaturized, self-powered solution for wearable electronics and smart textiles [28]. A PEDOT-bridged hydrogel–foam interface sensor with dual-conductive networks was designed by Lan et al. that achieves stable electron transmission under strain, delivering high sensitivity (27.8 kPa^{-1}) and 3.1 mW m^{-2} power density, advancing flexible, self-powered wearable electronics by overcoming interfacial charge transfer limitations [29]. Xu et al. fabricated a hydrogel yarn-based supercapacitor–sensor integrating PVA@P(AA-ANi)-SDS yarn and rGO-modified cotton film achieves high energy density (37.3 Wh kg^{-1}), excellent flexibility (300 % stretchability), and sensitivity (25.75 kPa^{-1}), offering a robust and comfortable solution for wearable energy storage and pressure sensing [30]. While new nanostructured materials and device architectures have been the focus of recent developments in high-performance energy harvesting, this work relies upon showcasing an inexpensive, reusable textile platform that combines energy harvesting with sensing [31–33]. This paves the way of a sustainable path that not only achieves competitive performance but also promotes circular economy concepts for useful, environmentally friendly applications by using waste cotton and recycled polyethylene (PE) into both S-S and L-S TENGs.

In the present study, we have repurposed waste cotton textiles by modifying their surface characteristics, from hydrophilic to hydrophobic, using a novel immersion method. These treated waste fabrics were then used to fabricate two distinct types of TENGs: (i) a solid–solid TENG (S-S TENG) and (ii) a liquid–solid TENG (L-S TENG). The S-S TENG operated in single-electrode mode, which was utilized to power small electronic devices. Furthermore, the TENG was attached to the ankle area under the sock for evaluation of a wide range of human activities and electrical responses arising from normal conditions, along with unusual conditions such as twisting, stretching, or bending. These motions were captured and fed into an artificial neural network to determine the accuracy of the sensor during both normal and unusual human motions.

In addition, the L-S TENG was designed using a PE coated waste cotton textile layer as a solid and deionized (DI) water as a liquid. The bottom electrode L-S TENG was then evaluated for a range of electrical outputs and self-powered sensing of adultered milk samples; this application was selected due to the urgent need for simple, cost-effective, and portable methods to detect food adulteration, especially in milk, which is a widely consumed and commonly tampered product. Utilizing a TENG-based approach enables on-site detection without reliance on external power sources, aligning with current trends in sustainable and point-of-care diagnostics. Our results suggest that the TENG, based on reused materials, has flexible working modes, and this new approach provides a low-cost, flexible, and eco-friendly platform for multifunctional energy harvesting and self-powered sensing, advancing circular economy principles and enabling new applications in healthcare, food safety, and wearable electronics.

2. Experimental techniques and material processing

The PE coated cotton textile was prepared using a dissolution and immersion method, utilizing recycled PE gloves as the raw material. Initially, used PE gloves from the laboratory were thoroughly cleaned and then cut into small pieces (1 × 1 cm^2). A measured amount of PE pieces (5.656 g) was added to a beaker containing 100 mL of toluene. The mixture was then stirred and heated at 100 °C for 30 min to facilitate the dissolution of the PE. After the heating process, any undissolved impurities were removed, resulting in a clear and uniform PE solution. The used cotton textile, which had been cleaned and dried, was then immersed for a few seconds in the solution above and kept in an oven at 50 °C for drying. The resulting cotton is therefore termed *PE-coated cotton.*

For the fabrication of the TENG, the working mode was selected as a single electrode mode with a bottom electrode in both S-S and L-S configurations. In the case of the S-S TENG, the PE-coated waste textile acted as a triboelectric layer, and a PDMS elastomer was selected as the opposite triboelectric layer. For the L-S TENG, PE-coated waste is used as a solid layer, while the DI water is used as a liquid contact. The active area of TENG was fixed at 4 cm × 3 cm for both devices, and aluminum tape was used as the bottom conductive electrode in the device setup. The PE-coated waste textile layer and aluminum layers were securely attached to the lower polyethylene terephthalate (PET) sheet. To enable electrical measurements, wires were connected to the aluminum electrodes, completing the assembly for performance testing.

Contact angle measurement of the surface of the PE-coated waste cotton textile and the waste cotton textile was undertaken using a contact angle goniometer (Ossila, UK). The surface morphology was examined using the scanning electron microscope (SEM) (SU-8020, Hitachi), and elemental mapping was carried out using an Oxford EDS spectrometer. The X-ray diffraction (XRD) pattern of the samples was obtained using the XRD diffractometer (M/S Malvern Panalytical, Netherlands), having Cu-Kα radiation and a rate of 3°/min. The 3D surface roughness was measured using an AFM (XE-100, Park Systems, Korea) with a lock-in amplifier and a silicon tip coated in Pt/Cr. Fourier Transform Infrared (FT-IR) spectra were measured using an FT-IR spectrometer (Thermo Fisher Nicolet iS5, USA). Three-dimensional dispersibility analysis was carried out using Synchrotron Radiation X-ray Tomographic Microscopy (SR-XTM) at the Synchrotron Light Research Institute (SLRI), Thailand, on beamline 1.2 W. X-ray images were captured over a rotational range of 0 to 180°, with data collected at every 0.1° step. To assess the performance of solid-solid TENG, a LinMot 1100 linear motor was used, allowing accurate regulation of motion frequency and displacement through dedicated control software. Real-time voltage and current outputs were measured using a Keithley

6514 programmable electrometer, with signal acquisition and monitoring carried out using the LabVIEW interface. MATLAB R2018a was used to create the feed-forward neural network for exercise movement detection.

3. Results and discussions

Fig. 1 shows the step-by-step procedure to fabricate the PE-coated waste cotton textile to create active triboelectric materials for the fabrication of TENG-based energy harvesters and sensors. The *PE-coated cotton* textile, which was utilized as an active triboelectric layer for the fabrication of a single-electrode TENG. The superhydrophobic nature of the PE-coated waste textile was confirmed by measuring the contact angle, which was 138°

Fig. 2(a, b, c, and d) shows SEM and EDS elemental mapping of waste cotton textile and PE-coated waste cotton textiles. In Fig. 2(a), the SEM of waste cotton textile displays a fibrous, porous structure, indicating exposed cellulose fibers. In contrast, Fig. 2(b) shows the PE-coated cotton textile with a smooth and dense surface, confirming successful polymer coating. Images Fig. 2(c) and (d) present EDS mapping for carbon (C) and oxygen (O). In Fig. 2(c), both C and O are uniformly distributed on the surface of the waste textile layer. In Fig. 2(d), the C signal is dominant, while O is reduced, confirming the presence of a polyethylene (C-rich) layer over the cotton substrate. Fig. 2(e) shows the XRD pattern of the waste cotton textile and the coated cotton textile. The pure cotton textile sample shows distinct diffraction peaks at $2\theta \approx 14.8°$, 16.6°, 22.7°, and 34.5°, corresponding to the $(1\bar{1}0)$, (110), (200), and (004) planes of cellulose structure, indicating its native crystalline nature [34]. In contrast, the PE-treated cotton exhibits a broad and less intense peak at approximately 22°, with diminished intensity in other regions, suggesting that the polyethylene coating disrupts the crystalline order of the cotton fibers. The reduced intensity and peak broadening confirm successful PE deposition, which masks the characteristic cellulose peaks.

The 3D volumetric imaging of the waste textile and PE-coated waste textile was obtained using XTM, as shown in Fig. 2**(f).** The waste cotton textile exhibits a porous, fibrous structure with visible voids and open channels. In contrast, PE-coated waste textile displays a dense, uniform layer, indicating successful PE coating, which fills the gaps and smoothens the surface. The surface roughness was determined using AFM, as shown in Fig. 2**(g),** which shows that the PE-coated waste textile roughness (R_q ~ 0.439 μm) was greater than that of the waste textile (R_q~ 0.185 μm). FT-IR spectroscopy was employed to examine the chemical structure and identify functional groups present on the waste cotton textile before and after surface modification, as shown in Fig. 2**(h)**. After applying the PE layer, characteristic absorption bands appeared at 2918 and 2850 cm^{-1}, corresponding to the asymmetric and symmetric stretching of C–H bonds [35]. These spectral features confirm the successful introduction of PE coatings on the cotton fiber surfaces.

Fig. 3**(a)** highlights the contact angle test of the waste cotton textile, and Fig. 3(b) the PE-coated waste textile, and further under various conditions, such as on different days Fig. 3**(c)** and at various pH levels **(d).** From Fig. 3**(a),** it was observed that the pure cotton textile was hydrophilic, and after 3 s, the DI water was absorbed. However, in Fig. 3 **(b)**, it can be seen that after the PE coating onto the waste textile. Ensuring the durability of the hydrophobic layer on the reused cotton textile is essential for its effective use in real-world applications, since it is likely to be exposed to diverse environmental conditions. The PE-coated cotton fibers maintained water contact angles above 135°, indicating excellent hydrophobic stability even after days of repeated testing. To further assess the durability of the hydrophobic layer, the PE-coated waste cotton textile samples were submerged in various media, including aqueous solutions with pH levels of 4, 7, and 9, which shows the superhydrophobic nature of the sample remains after 12 h of immersion in a range of pH solutions.

Fig. 4(a and b) highlights the working mechanism of the solid–solid and liquid-solid TENG. Fig. 4(a) illustrates the working mechanism of a single electrode mode TENG. When the two surfaces come into contact, electrons are transferred due to the difference in triboelectric polarity (one tribopositive layer (PE-coated waste cotton textile) and the tribonegative layer (PDMS), generating opposite surface charges. Upon separation, an electric potential is created between the electrodes, leading to electrons flowing through the external circuit, thereby producing a current. The flow of electrons stops, and it reaches equilibrium when both tribolayers are completely separated. As the tribonegative layer returns to make contact, the potential difference reverses, and electrons flow in the opposite direction. This periodic contact and separation cycle results in the generation of an alternating current (AC) based on the triboelectric and electrostatic induction principles. Fig. 4**(b)** illustrates a bottom electrode liquid-solid TENG operating mechanism. The triboelectric effect leads to charge transfer at the interface as a water droplet comes into contact with a solid surface (PE-coated cotton waste textile). Normally, the solid layer gains negative charges, while the liquid gains positive charges. A potential difference is thereby created when the

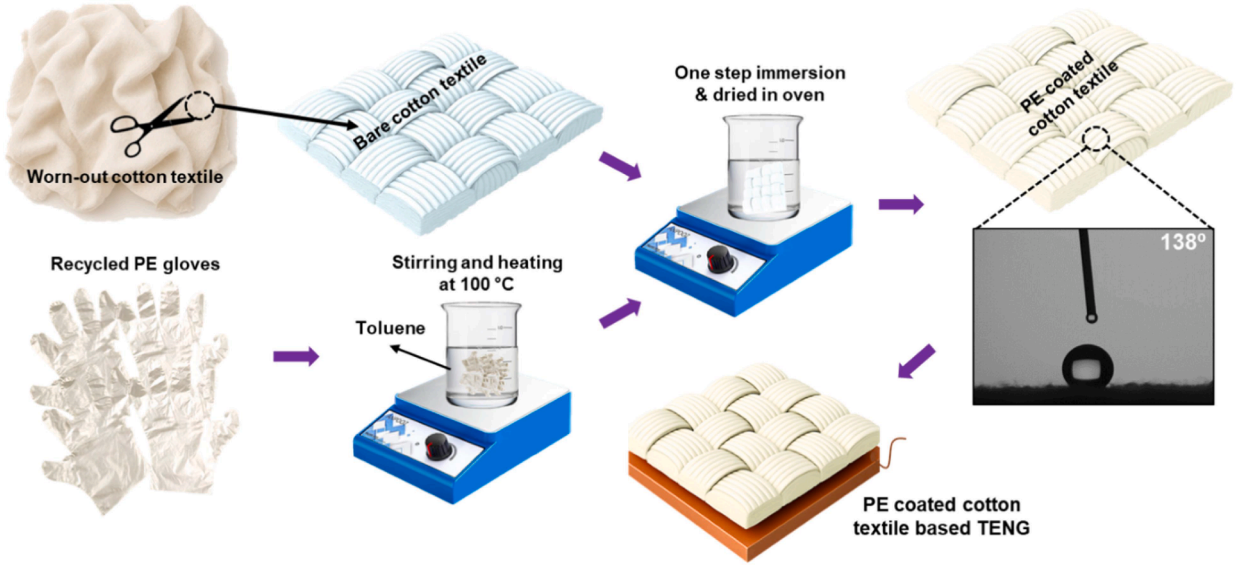

Fig. 1. Systematic step-by-step procedure of waste collection and coating techniques for the waste cotton textile and polyethylene (PE) gloves.

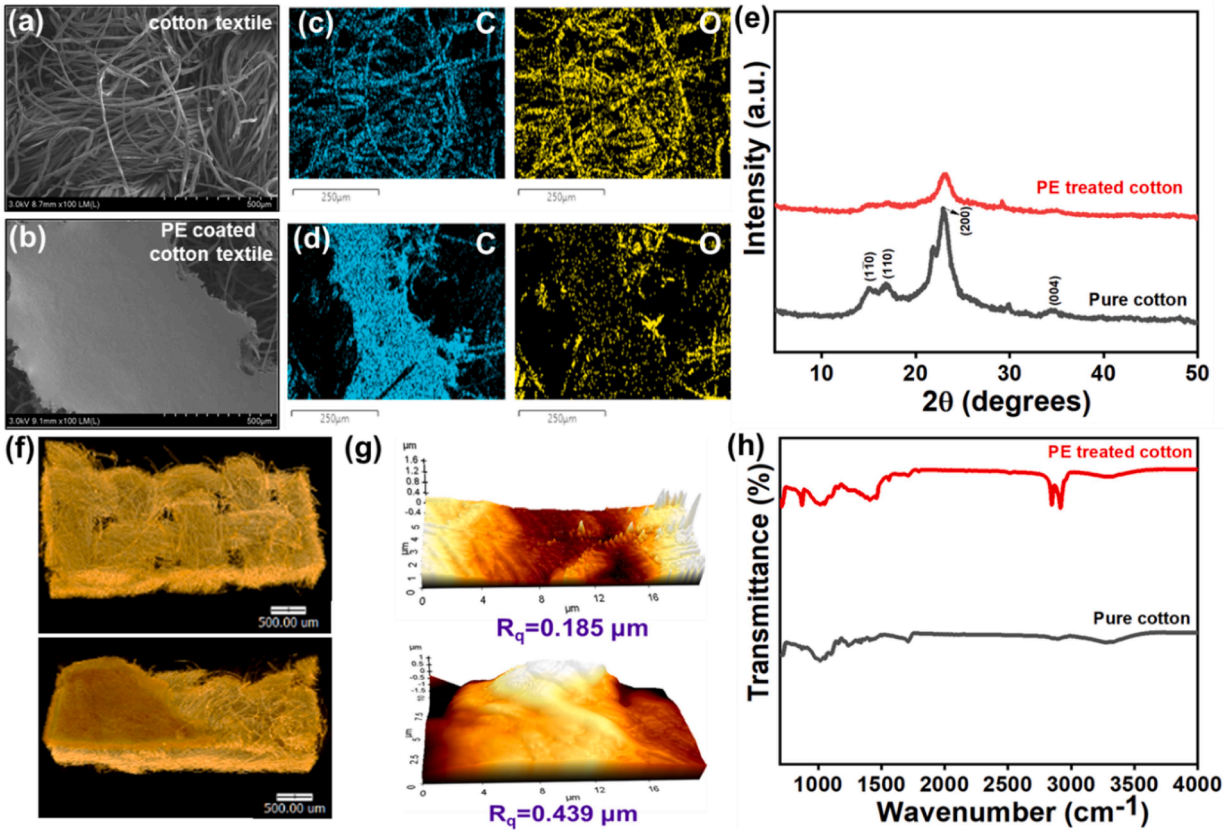

Fig. 2. (a, b) Surface morphology of the waste cotton textile and polyethylene (PE)-coated cotton textile, (c, d) elemental color mapping of the waste cotton textile and PE-coated cotton textile, (e) X-ray diffraction pattern of the waste cotton textile and PE-coated cotton textile, (f) 3D visualized (SR-XTM) images of waste cotton textile and PE-coated cotton textile, (g) AFM 3D images waste cotton textile and PE-coated cotton textile, and (h) FT-IR spectra of waste cotton textile and PE-coated cotton textile.

droplet rolls or moves across the surface, causing a dynamic redistribution of charges. Electrons flow in the external circuit as a result of this movement. An alternating current is created when the droplet separates, since the reverse potential pushes the electrons in the other direction. When this cycle is repeated, the liquid–solid interaction produces an electric output.

Fig. 5 presents the electrical output of a solid-solid TENG for a range of conditions. In Fig. 5**(a) and (b),** the voltage and current outputs are compared when PDMS is used as a negative triboelectric layer, while either waste cotton textile (W-textile) or PE-coated waste cotton textile (C-textile) is used as an opposite triboelectric positive layer in the TENG. The PDMS/C-textile pair exhibits a significantly higher voltage (250 V) and current (1.01 µA) than the PDMS/W-textile combination, confirming enhanced triboelectric performance after modification and coating with PE; this can also be due to enhanced surface roughness of the triboelectric layer due to coating of PE onto the waste cotton textile. Fig. 5**(c)** shows the charge output, with consistent charge peaks (~21 nC), indicating stable and repeatable charge generation. In Fig. 5**(d) and (e),** the voltage and current outputs of the TENG based on the coating C-textile are tested against different triboelectric layers: glass, PDMS, and polyurethane (PU) foam. The PDMS/C-textile combination yields the highest output, demonstrating optimal material pairing. The electrical output drops when using glass and PU foam, reflecting weaker triboelectric interactions. Fig. 5**(f)** illustrates long-term durability testing, where the voltage output remains stable for 1500 s under continuous operation.

Fig. 6**(a)** shows that the voltage output increases with load resistance, reaching a maximum at 10^9 Ω, indicating improved potential with higher resistance, following Ohm's law, since the flow of current is restricted. The highest power generated by the PDMS/C-textile TENG was recorded as 83.7 µW, where this peak performance is achieved at an optimal load resistance of 500 MΩ when subjected to a compression force of 5 N and an operating frequency of 2 Hz is shown in Fig. 6**(b)**. Fig. 6**(c)** shows the capacitor charging profiles for a range of storage capacitances, showing faster voltage rise for lower capacitance (2.2 µF) and slower rise for larger capacitances (47 µF), due to higher energy storage capacity. Fig. 6**(d)** shows that the stored charge increases with capacitance, indicating greater energy accumulation potential in larger capacitors. Fig. 6**(e)** shows the 2.2 µF capacitor shows cyclic both charging and discharging behavior, confirming stable energy storage and release over repeated cycles. The AC signal of TENG was converted to a DC signal using the bridge rectifier circuit. Furthermore, a 10 µF capacitor was charged to 3.3 V as shown in Fig. 6**(f),** leading to the illumination of LEDs (see inset), demonstrating a practical, sustainable power source by the TENG energy harvester.

Fig. 7 demonstrates the use of a TENG for motion detection and injury monitoring. Fig. 7**(a)** shows voltage signals for foot bending at angles of 0°, 45°, and 90°, indicating distinguishable output patterns. Fig. 7**(b)** compares normal ankle movement, as well as less normal movements such as a sprain, revealing significantly different voltage profiles. Fig. 7**(c)** shows a differentiation between regular and twisted foot bending, with twisted motion producing higher, more irregular signals. On integrating an Artificial Neural Network (ANN) with a TENG, intelligent interpretation of complex motion or physiological signals for real-time decision-making is possible [36–38]. An ANN-based method has been created in this study to automatically assess the quality of movement patterns in patients receiving physical therapy for injuries to their lower limbs. First, different knee motions are gathered as information, and various kinds of knee movements are included in the input data. A confusion matrix was used to demonstrate the classification

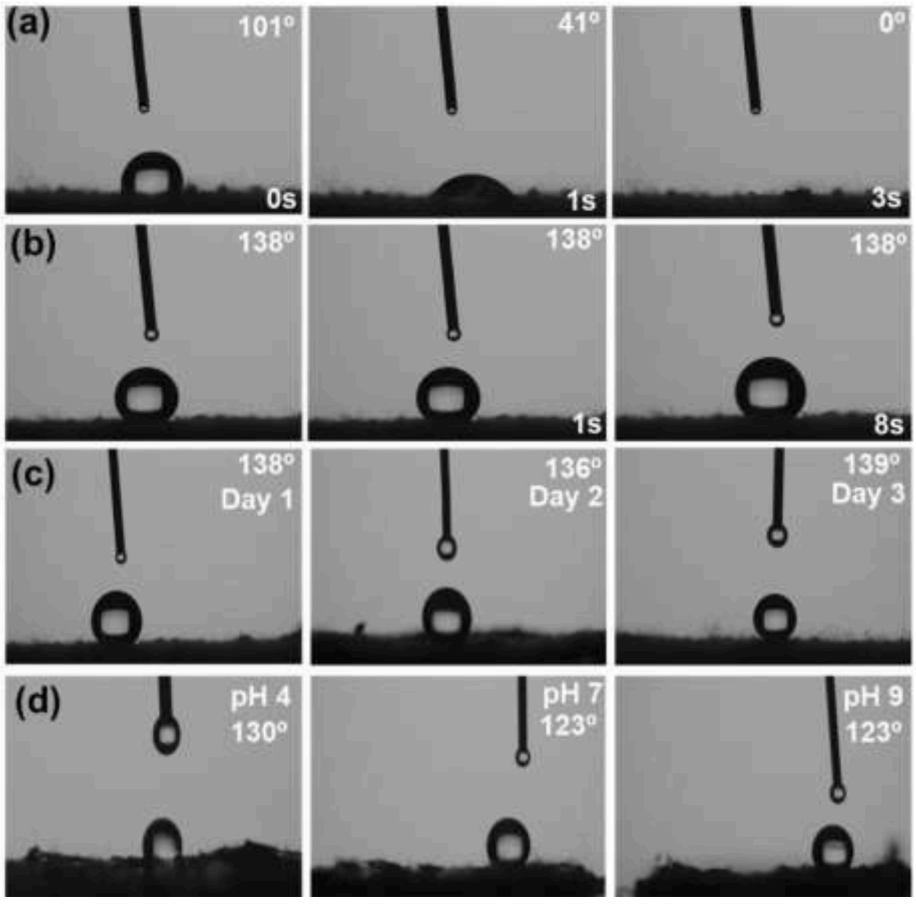

Fig. 3. (a) Contact angle study of the waste cotton textile from 0 to 3 s, (b) contact angle study of the PE-coated waste cotton textile from 0 to 8 s, (c) contact angle study of the PE-coated waste cotton textile at different days, and (d) contact angle study of the PE-coated waste cotton textile at various pH.

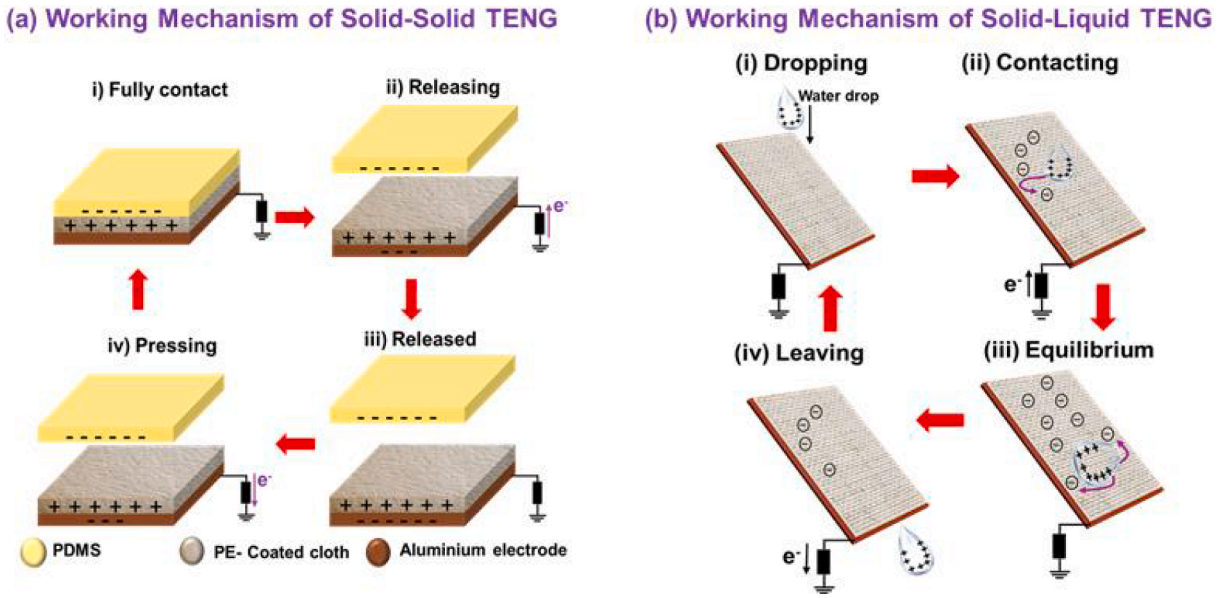

Fig. 4. Working mechanism of the (a) solid–solid TENG, and (b) liquid-solid TENG.

model's performance. Clinicians using ANN-based rehabilitation can make well-informed judgments regarding patient progress or required therapy modifications, using the confusion matrix to evaluate the precision and dependability of the system's movement perception. The confusion matrix analysis shows that the ANN model is highly capable of categorizing lower limb movement patterns among patients receiving physical therapy. The diagonal cells contain the datasets that have been correctly classified, whilst the off-diagonal cells contain the datasets that have been wrongly classified. The overall percentage of instances that were correctly classified (green) and cases that were wrongly classified

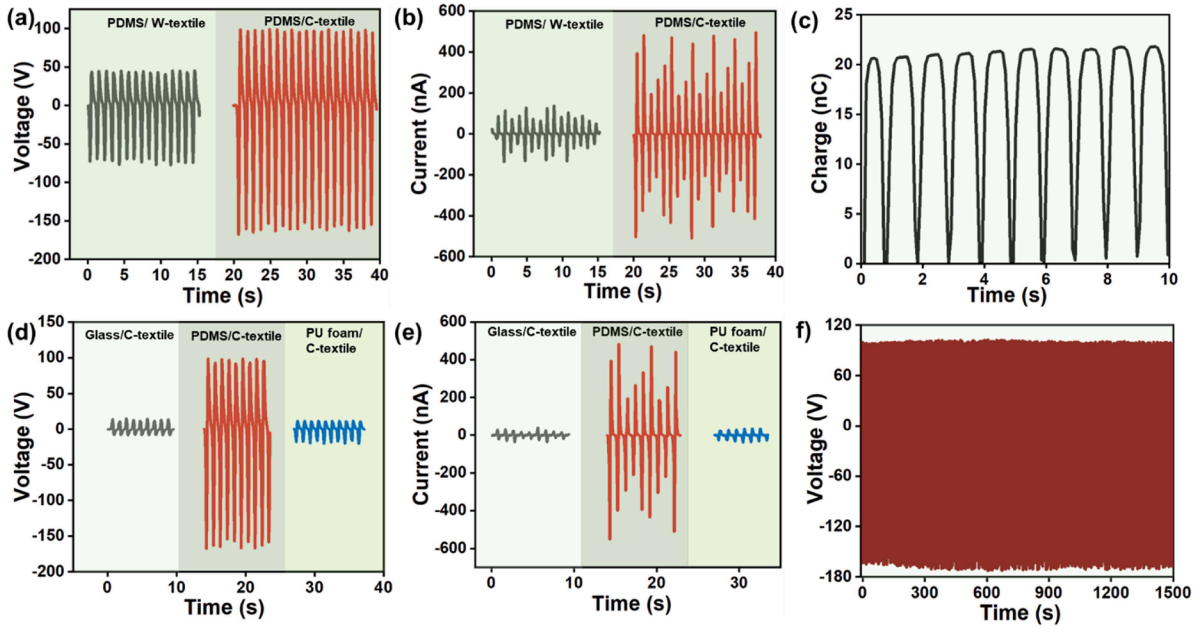

Fig. 5. (a) Voltage comparison of the waste cotton textile and PE-coated cotton textile with fixed opposing layers of PDMS, (b) current comparison of the waste cotton textile and PE-coated cotton textile with fixed opposing layers of PDMS, (c) charge delivered by PE-coated cotton textile/ PDMS TENG, (d) voltage delivered by PE-coated cotton textile with varied opposing layers, (e) current delivered by PE-coated cotton textile with varied opposing layers, and (f) long-term stability of the PE-coated cotton textile/ PDMS TENG.

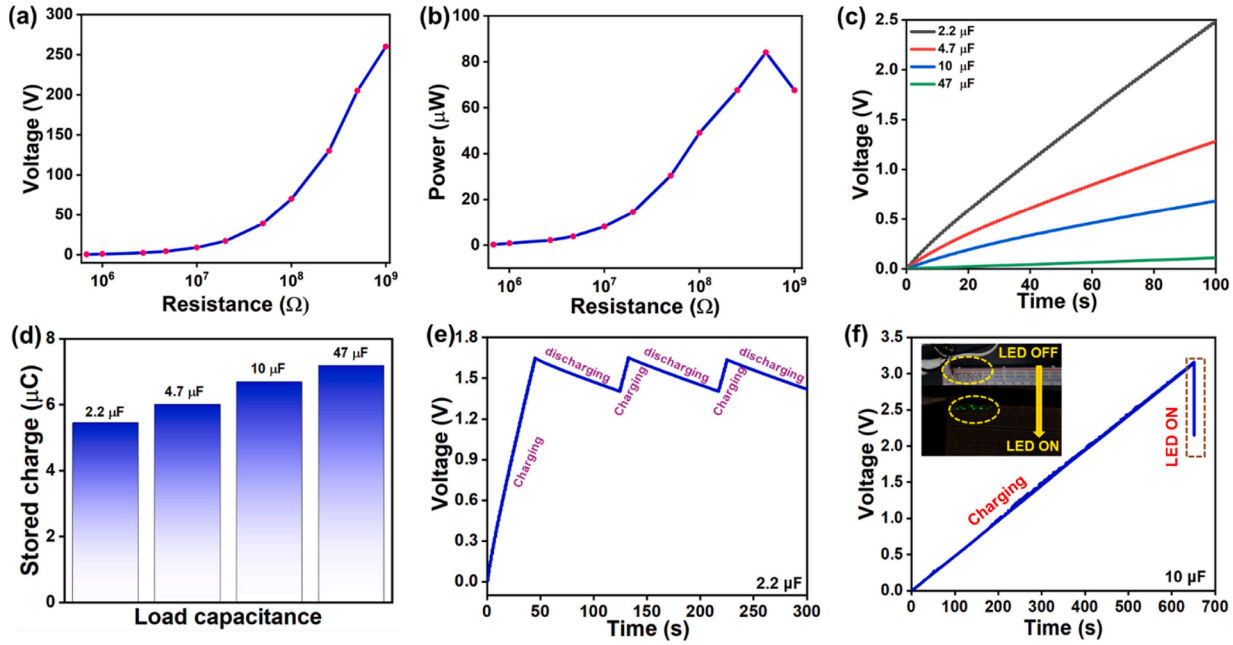

Fig. 6. (a) Voltage of PE-coated cotton textile/PDMS TENG for various load resistances, (b) power output of PE-coated cotton textile/PDMS TENG at various load resistances, (c) various capacitor charging with time plot using PE-coated cotton textile/PDMS TENG for 100 s, (d) calculated charge stored in each capacitor, (e) charging and discharging plot of the 2.2 μF capacitors, (f) charging of the 10 μF PE-coated cotton textile/PDMS TENG for powering LEDs.

(red) is displayed in the blue cell at the bottom right. 98.4 % (239 out of 243) of the test individuals were correctly classified, whereas 1.6 % (4 out of 243) were wrongly classified, as shown by the total confusion matrix in Fig. 7**(d)**. The complete dataset is divided into training, testing, and validation sets and converted into 1D arrays in order to train an ANN. 70 % of the data is used for training, 15 % for testing, and 15 % for validation. In this case, 171 of the 243 voltage samples collected are used to train the network. The network is tested and validated using each of the 36 samples. **Fig. S1** describes the optimal validation performance of the network as shown by performance graphs. The validation's efficacy is 3.2923×10^{-7}. To reduce this risk, specific precautions were implemented. The model did not overfit to the training data, as evidenced by the training and validation curves in **Fig. S1**, which showed a consistent, parallel drop without noticeable divergence. The schematic in Fig. 7**(e)** illustrates the process: signal generation by TENG, data acquisition, machine learning classification, and output decision-making. The ANN model effectively classifies lower limb movement patterns in physical therapy patients, achieving 98.4 %

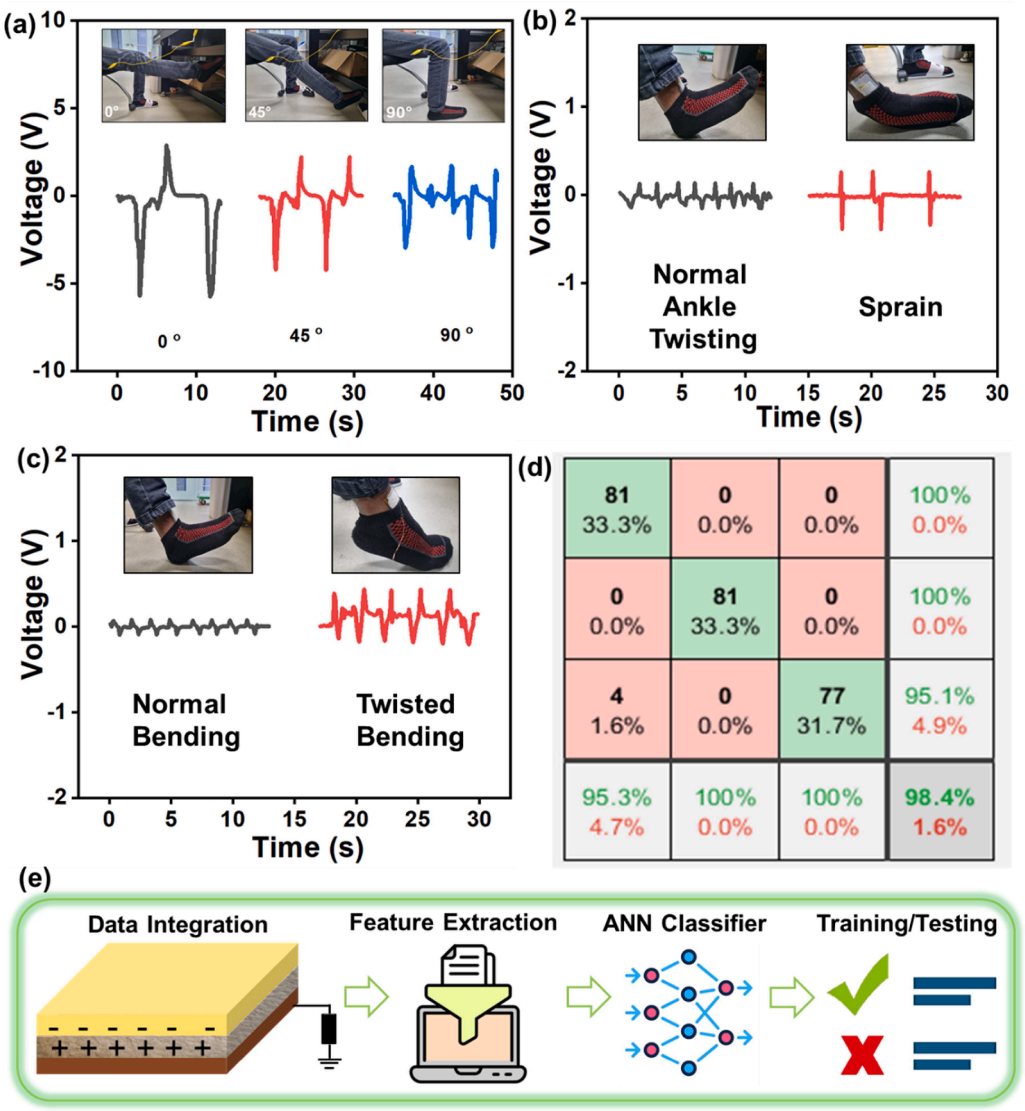

Fig. 7. (a) Voltage produced by TENG for monitoring knee hyperextension, (b) voltage produced by TENG for monitoring ankle sprains, (c) output voltage of normal flexion and twisted flexion and extension of the ankle joint, (d) confusion matrix to predict the accuracy of sensor during monitoring of exercise activity, (e) flowchart for TENG data for exercise techniques recognition based on ANN algorithm.

accuracy. The approach reliably distinguishes normal from abnormal movements, with only 4.6 % misclassified as aberrant. This highlights ANN's potential in clinical decision support for rehabilitation monitoring and progress evaluation.

The L-S TENG configuration was designed using the PE-coated waste cotton textile and DI water as the liquid droplet (see Fig. 4**b**). Electrostatic induction is the working mechanism that results in a lower output performance for a bottom-electrode layout. Fig. 8**(a and b)** shows the voltage and current of the L-S TENG at various tilt angles with a fixed water drop height of 3 cm. The effect of different tilt angles (30° to 55°) on device performance was investigated. An enhanced output was observed as the tilt angle was increased, which led to better water contact and spreading onto the triboelectric solid layer and an increase in the charge accumulation across the PE-coated waste textile layer. At a 45° tilt, the quicker droplet motion shortens electron flow time, thereby enhancing the electrical output. **Fig.S2 a** shows the output of the L-S TENG at various pH levels of the liquid drop on the L-S TENG. The concentration of H^+ is higher at pH 4, and the concentration of OH^- will be higher at pH 11. This influences the surface charge density, ionic strength and leads to a reduction in electrical output whereas in pH 7, it is a neutral balance of H^+, OH^-. **Fig. S2 b** shows the liquid-solid interface electric double layer model formation, which suggests that electron transfer predominantly governs the charge transfer mechanism between PE-coated cotton textile and water. Specifically, electrons accumulate progressively on the solid PE-coated cotton textile surface, generating a sustained electrical output, while the liquid water phase continuously loses electrons throughout the process.

The long-term stability of the output was achieved by dropping several water drops for over 300 s, and the amplitude of the voltage output remains constant in Fig. 8**(c)**. The water drop speed was varied from slow to fast, which shows that at various frequencies (slow drop frequency=0.3 Hz, fast drop frequency = 1.72 Hz), the voltage remains constant as the charge generated by the water as it makes an impact with the solid layer is also constant**;** Fig. 8**(d).** The charge retention of the L-S TENG was investigated by dropping the water droplets upon the solid layer for a longer period of 120 s, as shown in Fig. 8**(e)**, where the saturated charge generation is seen to be 1.3 nC. Fig. 8**(f)** shows the power output of L-S TENG at various load resistances, where the highest power of 45 nW at 50 MΩ was obtained. Fig. 8**(g)** showcases the 3D illustration of the bottom electrode L-S TENG and digital image of the water droplet falling, contacting, or impacting upon the solid PE-coated cotton waste textile layer and subsequently sliding down the device

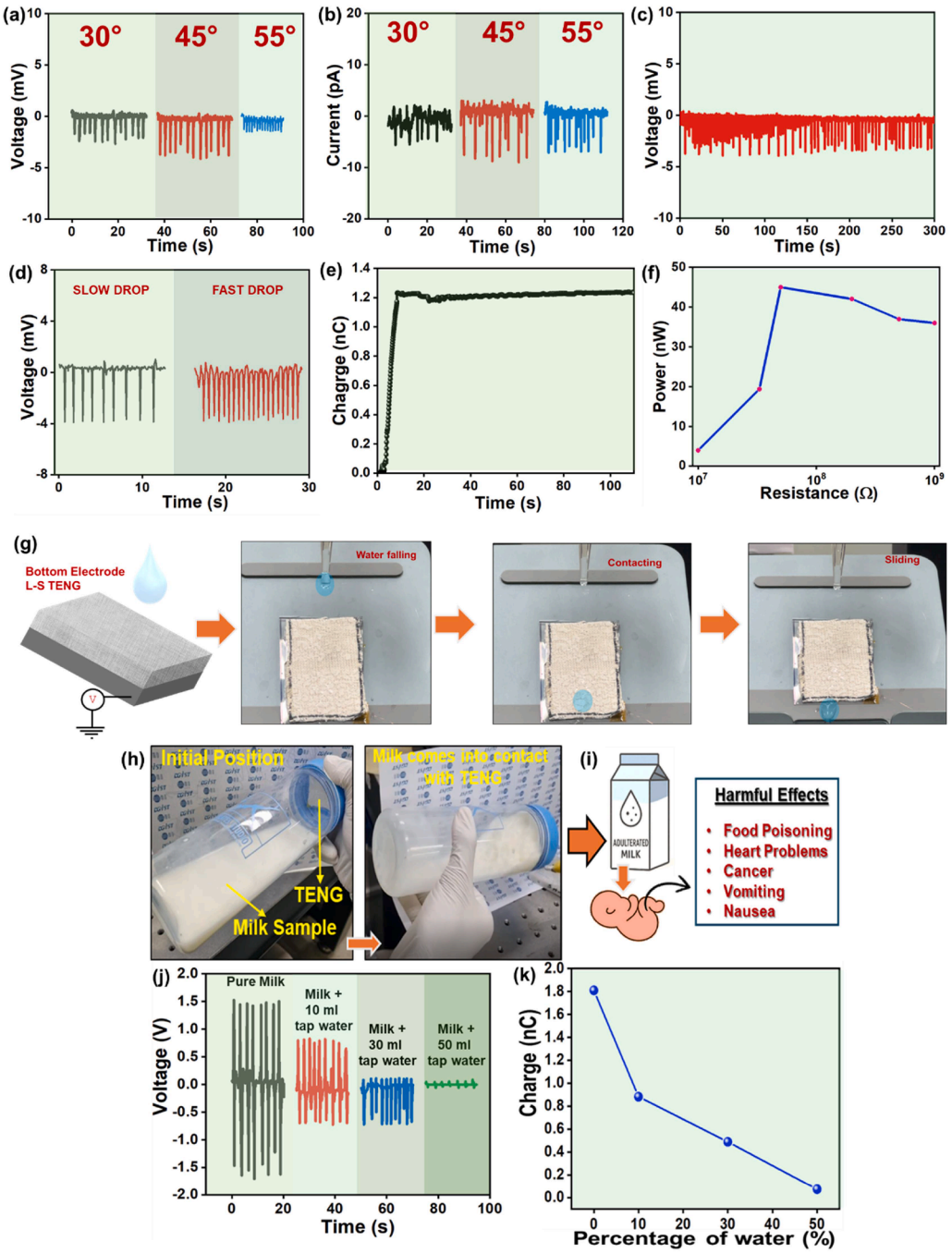

Fig. 8. (a, b) Voltage and current generated by PE-coated cotton textile-based TENG upon impact by deionized water, (c) long-term stability of the liquid–solid TENG based on PE-coated cotton textile, (d) voltage generated by PE-coated cotton textile-based TENG upon slow drop and fast drop of deionized water, (e) charge retention of the PE-coated cotton textile-based TENG, and (f) power generated by the liquid-solid TENG at various load resistances, and (g) digital image of the liquid–solid with bottom electrode showcasing the water falling, contacting and sliding, (h) digital image of TENG being attached inside a bottle cap and liquid (milk) initial position and during liquid-solid interface contact, (i) illustration of harmful effects of adulterated milk upon small babies, (j) liquid-solid TENG-based voltage output at various water % mixed in milk, and (k) corresponding charge (Q) generated by TENG when the TENG makes contact with milk.

structure. When a droplet touches a solid triboelectric layer (PE-coated cotton), it forms an electric double layer (EDL). As the water droplet detaches from the triboelectric layer, a potential difference is produced between the bottom electrode and ground, driving electron flow until charge balance is achieved. Repeated droplet contact with a solid triboelectric layer maintains a constant electrical output.

Fig. 8**(h)** shows the digital images of the portable setup of L-S TENG integration with a bottle (at an initial stage and when the milk touches the L-S TENG) for evaluation of milk adulteration to assess food safety. Fig. 8**(i)** shows the importance of self-powered sensors for the detection of milk adulteration. Since their immunological and digestive systems are still developing, infants are especially susceptible to the negative consequences of milk adulteration. In addition to compromising nutritional integrity, adulterants, including tap water, urea, starch, or detergents, can result in dehydration, food poisoning, gastrointestinal infections, vomiting, or long-term organ damage [39]. In addition, adulterants may contain infections or chemical residues that cause allergic reactions or long-term health problems in infants, such as metabolic disorders and developmental delays [40,41]. The fabricated L-S TENG device can sense the milk adulteration by simple phenomena

as when milk comes into contact with the solid triboelectric surface (e.g., PE-coated cloth), charge transfer occurs due to differences in their polarity and chemical potential. This results in electrostatic induction. Adulterants change the ionic strength, pH, and dielectric constant of milk, modifying the ion adsorption dynamics at the interface, thus altering the surface charge density. Fig. 8**(j)** shows the voltage output of the L-S TENG with various liquids such as pure milk (50 ml), milk (50 ml) +10 ml tap water, milk (50 ml) +20 ml tap water, and milk (50 ml) +30 ml tap water. There is a decline in voltage that indicates a reduction in charge generation efficiency as a result of the altered physicochemical properties in adulterated milk. **Fig. S3 a** shows that the voltage output decreases from approximately 1.50 V to 0.045 V as varying amounts of tap water (0–30 mL) are added to a fixed 50 mL volume of milk. This result demonstrates that the TENG-based milk sensor can clearly distinguish between pure milk and milk diluted with tap water. **Fig. S3 b** illustrates the linear regression between voltage output and milk concentration (v/v%), revealing a sensitivity of 42 mV per % (v/v) milk. **Fig. S4** shows the voltage output of the L-S TENG with various sample of milk. Variations in milk fat content affect dielectric constant and ionic conductivity, altering triboelectric charge transfer at the L–S interface. Fig. 8**(k)** shows the charge generated by the L-S TENG when the pure as well as water-mixed milk touched the TENG device. The charge (Q) tends to decrease, which can be confirmed by the formula $Q = CV$, since if Q (charge) decreases, the voltage (V) also decreases if the capacitance (C) of the device remains constant. **Table T2** shows the comparison of the proposed L–S TENG based milk adulteration sensor with conventional techniques. The self-powered sensor is simple to construct, user-friendly, affordable, and portable, making it ideal for on-site applications. It operates without the need for specialized skills and provides immediate readings through dynamic changes in voltage or charge output using an electrometer readout.

4. Conclusions

In this work, we have developed a dual-mode energy harvesting system using waste polyethylene-coated cotton textiles for both solid–solid (S-S) and liquid-solid (L-S) triboelectric devices. The S–S TENG demonstrated high performance with an output voltage of 250 V, current of 1.01 μA, and peak power of 83.7 μW, which was able to effectively power small electronic components. The L–S TENG achieved a power output of 45 nW and exhibited consistent performance with water droplet impact and water sliding, demonstrating robustness under varying mechanical conditions. In addition, the system enabled intelligent motion recognition with 98.4 % accuracy by employing artificial neural networks. Furthermore, the L-S TENG-based sensor successfully detected milk adulteration levels for assessing food safety. These results emphasize the potential of modifying waste textiles to create efficient, low-cost, and eco-friendly materials for multifunctional nanogenerators and sensors. The integration of energy harvesting and real-time sensing paves the way for next-generation wearable electronics, smart healthcare monitoring, and environmental diagnostics, aligning with sustainability goals and the advancement of circular materials technology.

CRediT authorship contribution statement

Kushal Ruthvik Kaja: Writing – original draft, Formal analysis, Conceptualization. **Sugato Hajra:** Writing – original draft, Formal analysis, Conceptualization. **Swati Panda:** Formal analysis, Data curation. **Mohamed Belal:** Data curation. **Sangwoo Nam:** Investigation. **Phakkhananan Pakawanit:** Investigation. **Basanta Kumar Panigrahi:** Software. **Hamideh Khanbareh:** Writing – review & editing. **Chris Bowen:** Writing – review & editing, Visualization, Supervision. **Jaesok Yu:** Writing – review & editing, Visualization, Supervision, Methodology. **Hoe Joon Kim:** Writing – review & editing, Supervision, Project administration, Funding acquisition.

Declaration of competing interest

The authors declare that they have no known competing financial interests or personal relationships that could have appeared to influence the work reported in this paper.

Acknowledgement

This research is supported by the National Research Foundation of Korea (NRF) (RS-2024–00346135, RS-2024–00406674), and by the Basic Science Research Program through the National Research Foundation of Korea (NRF) funded by the Ministry of Education (RS-2025-25420118).

Supplementary materials

Supplementary material associated with this article can be found, in the online version, at doi:10.1016/j.rineng.2025.107111.

Data availability

Data will be made available on request.

References

[1] M.A. Abtew, D. Atalie, B.K. Dejene, Recycling of cotton textile waste: Technological process, applications, and sustainability within a circular economy, J. Ind. Text. 55 (2025), 15280837251348663.
[2] M.T. Rahaman, A.D. Pranta, M.R. Repon, M.S. Ahmed, T. Islam, Green production and consumption of textiles and apparel: Importance, fabrication, challenges and future prospects, J. Open Innov.: Technol., Mark. Complex. 10 (2024) 100280.
[3] U.N. Haq, S.M.R. Alam, Implementing circular economy principles in the apparel production process: reusing pre-consumer waste for sustainability of environment and econom, Clean Waste Syst 6 (2023) 100108.
[4] M.A.R. Bhuiyan, A. Ali, M. Mohebbullah, M.F. Hossain, A.N. Khan, L. Wang, Recycling of cotton apparel waste and its utilization as a thermal insulation layer in high performance clothing, Fashion Text. 10 (2023) 22.
[5] L. Sun, K. Fang, W. Chen, K. Liu, J. Zhu, C. Zhang, Fabrication of a novel superhydrophobic cotton by HDTMS with TiO2 supported activated carbon nanocomposites for photocatalysis and oil/water separation, Ind. Crops Prod. 189 (2022) 115836.
[6] X. Sha, L. Chen, Y. Jia, H. Zhao, S. Zuo, P. Yuan, G. Chen, Preparation and properties of sustainable superhydrophobic cotton fabrics modified with lignin nanoparticles, tannic acid and methyltrimethoxysilane, Chem. Eng. J. 499 (2024) 155797.
[7] P. Pransilp, M. Pruettiphap, W. Bhanthumnavin, B. Paosawatyanyong, S. Kiatkamjornwong, Surface modification of cotton fabrics by gas plasmas for color strength and adhesion by inkjet ink printing, Appl. Surf. Sci. 364 (2016) 208–220.
[8] S.O. Donkor, D. Sun, D. Bucknall, J. Buckman, Surface activation of cotton fabric with low-temperature air plasma treatment for metallic printing, Fibers Polym. 25 (2024) 4321–4332.
[9] S. Mishra, M. Rakshita, H. Divi, S. Potu, R.K. Rajaboina, Unique contact point modification technique for boosting the performance of a triboelectric nanogenerator and its application in road safety sensing and detection, ACS Appl. Mater. Interfaces 15 (2023) 33095–33108.
[10] P. Gajula, J.U. Yoon, I. Woo, J.W. Bae, Development of turbocharging-ability hybrid nanogenerators comprising bipolar PVDF-HFP/MXene electrospun composites, Small 21 (2025) 2407001.
[11] A. Bindhu, J.U. Yoon, I. Woo, P. Gajula, A.P. Arun, J.W. Bae, Enhanced charge holding capacity of PVDF nanofiber using NiO-CuO nanoparticles-based triboelectric nanogenerator for energy and wearable electronic applications, Adv. Sustain. Syst. 9 (2025) 2400604.
[12] M. Sahu, S. Šafranko, S. Hajra, A.M. Padhan, P. Živković, S. Jokić, H.J. Kim, Development of triboelectric nanogenerator and mechanical energy harvesting using argon ion-implanted kapton, zinc oxide and kapton, Mater. Lett. 301 (2021) 130290.
[13] S. Panda, S. Hajra, H.-G. Kim, P.G.R. Achary, P. Pakawanit, Y. Yang, Y.K. Mishra, H.J. Kim, Sustainable solutions for oral health monitoring: biowaste-derived triboelectric nanogenerator, ACS Appl. Mater. Interfaces 15 (2023) 36096–36106.
[14] J. Ahn, J.-S. Kim, Y. Jeong, S. Hwang, H. Yoo, Y. Jeong, J. Gu, M. Mahato, J. Ko, S. Jeon, J.-H. Ha, H.-S. Seo, J. Choi, M. Kang, C. Han, Y. Cho, C.H. Lee, J.-H. Jeong, I.-K. Oh, I. Park, All-recyclable triboelectric nanogenerator for sustainable ocean monitoring systems, Adv. Energy Mater. 12 (2022) 2201341.
[15] J.A.L. Jayarathna, K.R. Kaja, Energy-harvesting device based on lead-free perovskite, AI Comput. Sci. Robot. Technol. (2024).

[16] W.-G. Kim, D.-W. Kim, I.-W. Tcho, J.-K. Kim, M.-S. Kim, Y.-K. Choi, Triboelectric nanogenerator: Structure, mechanism, and applications, ACS Nano 15 (2021) 258–287.
[17] X. Xiao, G. Chen, A. Libanori, J. Chen, Wearable triboelectric nanogenerators for therapeutics, Trends Chem. 3 (2021) 279–290.
[18] J. Chen, Z.L. Wang, Reviving vibration energy harvesting and self-powered sensing by a triboelectric nanogenerator, Joule 1 (2017) 480–521.
[19] S. Panda, S. Hajra, Y. Oh, W. Oh, J. Lee, H. Shin, V. Vivekananthan, Y. Yang, Y. K. Mishra, H.J. Kim, Hybrid nanogenerators for ocean energy harvesting: mechanisms, designs, and applications, Small 19 (2023) 2300847.
[20] S. Hajra, K.R. Kaja, S. Panda, M.A. Belal, B.K. Panigrahi, P. Pakawanit, H.J. Kim, Waste based triboelectric nanogenerator for energy harvesting and self-powered sensors, J. Clean. Prod. 509 (2025) 145591.
[21] M. Navaneeth, S. Potu, A. Babu, B. Lakshakoti, R.K. Rajaboina, U. Kumar K, H. Divi, P. Kodali, K. Balaji, Transforming medical plastic waste into high-performance triboelectric nanogenerators for sustainable energy, health monitoring, and sensing applications, ACS Sustain. Chem. Eng. 11 (2023) 12145–12154.
[22] A. Panda, K.K. Das, K.R. Kaja, V. Gandi, S.G. Mohanty, B.K. Panigrahi, Low- cost high performance sustainable triboelectric nanogenerator based on laboratory waste, J. Met., Mater. Min. 35 (2025) e2226.
[23] W. Xu, H. Zheng, Y. Liu, X. Zhou, C. Zhang, Y. Song, X. Deng, M. Leung, Z. Yang, R. X. Xu, Z.L. Wang, X.C. Zeng, Z. Wang, A droplet-based electricity generator with high instantaneous power density, Nature 578 (2020) 392–396.
[24] Y. Wei, X. Li, Z. Yang, J. Shao, Z.L. Wang, D. Wei, Contact electrification at the solid–liquid transition interface, Mater. Today 74 (2024) 2–11.
[25] U. Pharino, K. Chaithaweep, S. Pongampai, N. Chanlek, S. Kothan, J. Kaewkhao, S. Hajra, H.J. Kim, W. Vittayakorn, S. Sriphan, N. Vittayakorn, A highly sensitive disease pre-screening approach for glycosuria: Triboelectric sensing at the liquid-solid interface, Chem. Eng. J. 508 (2025) 160901.
[26] Y. Mao, Y. Li, J. Xie, H. Liu, C. Guo, W. Hu, Triboelectric nanogenerator/supercapacitor in-one self-powered textile based on PTFE yarn wrapped PDMS/MnO_2NW hybrid elastomer, Nano Energy 84 (2021) 105918.
[27] L. Liu, Y. Li, M. Xu, R. Tao, Q. Zhong, X. Yang, S. Lan, J. Xie, G. Chen, Y. Mao, W. Hu, Hybrid tribo/piezoelectric nanogenerator textile derived from 3D interlocked parallel-arranged yarns for bio-motion energy harvesting and tactile sensing, Chem. Eng. J. 474 (2023) 145866.
[28] R. Tao, Y. Mao, C. Gu, W. Hu, Integrating all-yarn-based triboelectric nanogenerator/supercapacitor for energy harvesting, storage and sensing, Chem. Eng. J. 496 (2024) 154358.
[29] S. Lan, Y. Mao, B. Zhou, W. Hu, PEDOT-molecular bridging foam-hydrogel based wearable triboelectric nanogenerator for energy harvesting and sensing, Nano Energy 134 (2025) 110572.
[30] M. Xu, Y. Mao, W. Hu, All-hydrogel yarn-based supercapacitor wrapped with multifunctional cotton fiber for energy storage and sensing, Nano Energy 130 (2024) 110142.
[31] K. Xia, M. Yu, Highly robust and efficient metal-free water cup solid–liquid triboelectric nanogenerator for water wave energy harvesting and ethanol detection, Chem. Eng. J. 503 (2025) 157938.
[32] K. Xia, M. Yu, Y. Luo, Y. Ding, All-foam intrinsic triboelectric static and dynamic pressure sensor with a standardized DC/AC measurement method for industrial robots, Nano Energy 139 (2025) 110953.
[33] R. Liu, K. Xia, T. Yu, F. Gao, Q. Zhang, L. Zhu, Z. Ye, S. Yang, Y. Ma, J. Lu, Multifunctional Smart Fabrics with Integration of Self-Cleaning, Energy Harvesting, and Thermal Management Properties, ACS Nano 18 (2024) 31085–31097.
[34] J.R. Jayasinghe, A. Samarasekara, D. Amarasinghe. Synthesis and characterization of microcrystalline cellulose from cotton textile waste, 2020 Moratuwa Engineering Research Conference (MERCon), IEEE, 2020, pp. 187–192.
[35] Q. Zhang, Y. Cao, N. Liu, W. Zhang, Y. Chen, X. Lin, Y. Wei, L. Feng, L. Jiang, Recycling of PE glove waste as highly valuable products **for** efficient separation of oil-based contaminants from water, J. Mater. Chem. A 4 (2016) 18128–18133.
[36] H. Zhang, T. Liu, X. Zou, Y. Zhu, M. Chi, D. Wu, K. Jiang, S. Zhu, W. Zhai, S. Wang, Real-time data visual monitoring of triboelectric nanogenerators enabled by Deep learning, Nano Energy (2024) 110186.
[37] S. Duan, H. Zhang, L. Liu, Y. Lin, F. Zhao, P. Chen, S. Cao, K. Zhou, C. Gao, Z. Liu, A comprehensive review on triboelectric sensors and AI-integrated systems, Mater. Today (2024).
[38] C. Wang, T. He, H. Zhou, Z. Zhang, C. Lee, Artificial intelligence enhanced sensors-enabling technologies to next-generation healthcare and biomedical platform, Bioelectron. Med. 9 (2023) 17.
[39] M. Islam, N. Jhily, N. Priya, M. Hasan, J. Hossain, S. Chandra, S. Rahman, A. Islam, Dreadful practices of adulteration in food items and their worrisome consequences for public health: a review, J. Food Saf. Hygiene (2022).
[40] W.C. Li, C.F. Chow, Adverse child health impacts resulting from food adulterations in the Greater China Region, J. Sci. Food Agric. 97 (2017) 3897–3916.
[41] M.A. Al Mamun, B.K. Biswas, S.T. Tamanna, M.B. Islam, An Overview of Food Adulterants and their Health Impacts, Int. J. Sci. Res. Pub. (IJSRP) 11 (2021) 780–796.